Journal of Biomedical Optics

BiomedicalOptics.SPIEDigitalLibrary.org

MagIC, a genetically encoded fluorescent indicator for monitoring cellular Mg^{2+} using a non-Förster resonance energy transfer ratiometric imaging approach

Vadim Pérez Koldenkova
Tomoki Matsuda
Takeharu Nagai

SPIE.

MagIC, a genetically encoded fluorescent indicator for monitoring cellular Mg^{2+} using a non-Förster resonance energy transfer ratiometric imaging approach

Vadim Pérez Koldenkova, Tomoki Matsuda, and Takeharu Nagai*
Osaka University, Institute of Scientific and Industrial Research, Mihogaoka 8-1, Ibaraki, Osaka 567-0047, Japan

Abstract. Intracellular Mg^{2+} roles are commensurate with its abundance in the cell cytoplasm. However, little is known about Mg^{2+} subcellular dynamics, primarily due to the lack of suitable Mg^{2+}-selective tools to monitor this ion in intracellular compartments. To cope with this lack, we developed a Mg^{2+}-sensitive indicator—MagIC (indicator for Magnesium Imaging in Cell) —composed of a functionalized yellow fluorescent protein (FP) variant fused to a red-emitting FP serving as a reference, thus allowing ratiometric imaging of Mg^{2+}. MagIC expressed in mammalian cells is homogeneously distributed between the cytosol and nucleus but its fusion with appropriate targeting sequences redirects it to mitochondria or the endoplasmic reticulum. MagIC shows little interference by intracellular Ca^{2+} [$K_d(Mg^{2+}) = 5.1$ mM; $K_d(Ca^{2+}) = 4.8$ mM] and its kinetic properties ($k_{off} = 84\ s^{-1}$) approach those of indicator dyes. With MagIC, as reported previously, we also observed a cytosolic Mg^{2+} increase provoked by application of 50 mM $MgCl_2$ in the medium. This effect is, however, mimicked by 75 mM KCl or 150 mM D-sorbitol addition, indicating that it is a response to the associated hyperosmotic shock and not to Mg^{2+} itself. Our results confirm the functionality of MagIC as a useful tool for the long-awaited possibility of prolonged and organelle-specific monitoring of cellular Mg^{2+}. [DOI: 10.1117/1.JBO.20.10.101203]

Keywords: ratiometric imaging; genetically encoded fluorescent indicator; low affinity indicator; Mg_{2+}; indicator; hyperosmotic shock.

Paper 140863SSR received Jan. 1, 2015; accepted for publication Apr. 21, 2015; published online Aug. 5, 2015.

1 Introduction

Mg^{2+} is the most abundant intracellular divalent cation, which has a central role in the plant's light-absorbing molecule chlorophyll, and is an essential cofactor of adenosine triphosphate (ATP), the "energy currency" of the cell. Mg^{2+} plays an important role in the regulation of more than 350 enzymes,[1] particularly those dealing with DNA replication, transcription, and translation. Mg^{2+} has been proposed as a modulator of Ca^{2+} signaling[2] and a direct second-messenger role was recently reported for this ion during the activation of T-lymphocytes after antigen receptor stimulation.[3]

Total Mg^{2+} concentration in mammalian cells is in the 17 to 20 mM range,[4] however, most of it is considered to be bound to ATP, membranes, nucleic acids, proteins, or sequestered in intracellular organelles. Free Mg^{2+} concentration in cells is reported to be tightly regulated in the 0.25 to 1.5 mM range,[5] however, under hormonal or chemical stimulation, large Mg^{2+} fluxes are observed which do not drastically alter the cytosolic free Mg^{2+} level.[6] Several techniques, such as ^{31}P NMR, ion selective microelectrodes, and fluorescent Mg^{2+}-sensitive dyes, have been used to obtain information about free Mg^{2+} dynamics,[7] but only fluorescent dyes allow visualization of intracellular Mg^{2+} at the single cell level with relatively high spatial resolution. A great disadvantage of these dyes is, however, in most cases, their intensiometric nature meaning that measurements are affected by cell movement, focal plane shift, bleaching, or dye local concentration change, impeding prolonged monitoring of cellular Mg^{2+}. Few ratiometric Mg^{2+}-sensitive dyes exist (for example mag-fura-2),[8] but they require UV excitation which is harmful to the cell and requires a specialized optical setup.[7] Most Mg^{2+}-sensitive dyes also have high sensitivity for Ca^{2+} (with affinity constants for Ca^{2+} in the micromolar range), so they are predominantly used as low affinity Ca^{2+} indicators.[7] An exception is a recently developed class of Mg^{2+} indicators based on beta diketones (the KMG series), which display a high Mg^{2+}-over-Ca^{2+} selectivity [KMG-104 $K_d(Mg^{2+}) = 2.1$ mM, $K_d(Ca^{2+}) = 7.5$ mM].[9] An inconvenience of this group of dyes is, however, that they are also intensiometric thus hindering their use for prolonged imaging of intracellular Mg^{2+}.

Recently, the first family of genetically encoded indicators for Mg^{2+}, MagFRET, was reported. MagFRETs are based on the human centrin HsCen3 moiety flanked by the cyan fluorescent protein (FP), Cerulean, and the yellow FP, Citrine, as a Förster resonance energy transfer (FRET) donor and acceptor, respectively.[10] MagFRET variants showed affinity constants for Mg^{2+} in the 0.15 to 15 mM range, but the constructions with $K_d(Mg^{2+})$ close to the physiological Mg^{2+} range (MagFRET1, 2, 7, 8) also displayed a relatively high affinity for Ca^{2+} [$K_d(Ca^{2+})$] in the 10 to 50 μM range), thus potentially requiring attention when Ca^{2+} interference is possible. Expression of MagFRET1 in HEK293 cells without targeting sequences

*Address all correspondence to: Takeharu Nagai, E-mail: ng1@sanken.osaka-u.ac.jp

1083-3668/2015/$25.00 © 2015 SPIE

resulted, as in the case of Mg^{2+}-sensitive dyes, in cytosolic staining with a nonlabeled nucleus. But perhaps the main uncertainty regarding these indicators' functionality comes from the apparent insensitivity to several stimuli previously reported to increase free cytosolic Mg^{2+} [10] although, on the other hand, Mg^{2+}-dependent ratio changes were further confirmed when cells were permeabilized and high concentrations of Mg^{2+} or ethylenediaminetetraacetic acid (EDTA) were applied.

In our attempt, we developed an indicator for Mg^{2+} based on another non-FRET reporting mechanism. For our indicator, we used a novel FP functionalized to sense Mg^{2+} in the millimolar range. By addition of a second reference, FP, we conferred ratiometric properties to the indicator, thus making it insensitive to local variations in the fluorescence intensity caused by cell movement or defocusing. Different from other available Mg^{2+} indicators to date, our sensor, which we have called MagIC (indicator for Magnesium Imaging in Cell) localizes both in the cell nucleus and in the cytosol, allowing simultaneous imaging of Mg^{2+} in these compartments. In the present work, we have characterized this novel sensor and employed it for monitoring cytosolic Mg^{2+} under different conditions.

2 Materials and Methods

2.1 *Plasmid Construction, Protein Expression, and Purification*

Three residues in circularly permuted (cp) 173Venus were replaced using the approach previously described by Sawano and Miyawaki,[11] to obtain (S220E, S31D, Q33E)-cp173Venus. The sequence encoding this Venus variant was amplified using primers containing *Xho*I (forward) and *Eco*RI (reverse) restriction sites, and the open reading frame (ORF) was cloned into $pRSET_B$ vector (Invitrogen, Carlsbad, California). ORFs of reference FPs were amplified using primers containing *Bam*HI (forward) and *Xho*I (reverse) restriction sites and ligated in the vector containing the (S220E, S31D, Q33E)-cp173Venus between the *Xho*I restriction site and an upstream *Bam*HI restriction site [Fig. 1(b)]. In the final indicator (see below), spontaneous mutations—G4S [enhanced green fluorescent protein (EGFP) 177S], V89I (EGFP 18V), and Q142M (EGFP 72Q)—were found in the Mg^{2+}/Ca^{2+}-sensitive Venus moiety, so additional indicator variants were generated: (1) with reversed spontaneous mutations, (2) a variant holding all the acidic residues present in CatchER (F52E, T54E in the Mg^{2+}/Ca^{2+}-sensitive Venus, in addition to those shown in Table 1),[12] and (3) the reversed mutant holding only the five negatively charged residues of CatchER in the original cp173Venus moiety. All these mutations were introduced following the approach proposed by Sawano and Miyawaki[11] and the subsequent construction process was identical to that described above.

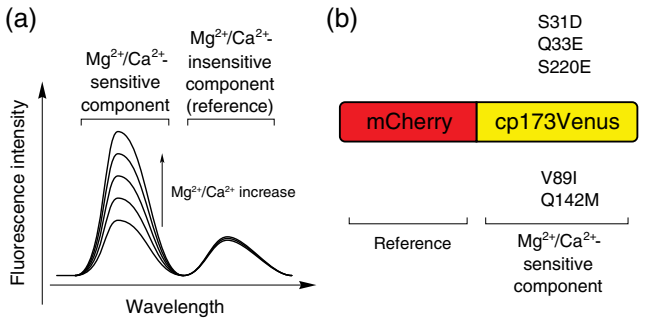

Fig. 1 Working principle and schematic representation of MagIC. Mg^{2+} concentration changes are reported by the fluorescence intensity of Mg^{2+}/Ca^{2+}-sensitive cp173Venus variant, which is then compared to the Mg^{2+}/Ca^{2+}-insensitive (constant) reference fluorescence intensity of mCherry. (a) Working principle and schematic representation of spectral changes of the ratiometric non-Förster resonance energy transfer (FRET)-based indicator composed of Mg^{2+}-sensitive and reference moieties. Mg^{2+} increase is indicated by the arrow. (b) Structure of the indicator gene featuring mutations introduced in cp173Venus.

Table 1 Amino acid replacements in the cp173Venus variant used in MagIC and corresponding mutations in EGFP-based CatchER.[12]

CatchER	Mg^{2+}/Ca^{2+}-sensitive cp173Venus
S147E	S220E
S202D	S31D
Q204E	Q33E
F223E	—
T225E	—

Mg^{2+}/Ca^{2+}-sensitive cp173Venus also contains the following mutations relative to the original cp173Venus: V89I, Q142M (in cp173Venus numeration).

Protein expression was carried out using the JM109 (DE3) *Escherichia coli* strain. Culturing was performed in 1× lysogeny broth medium at 23°C for 60 h with continuous shaking at 150 rpm. The bacterial pellet obtained after centrifugation was resuspended in phosphate-buffered saline (PBS) and mechanically lysed. The cleared lysate was purified using a Ni-NTA column (Qiagen, Hilden, Germany) and then gel-filtered in a PD-10 column (GE-Healthcare, Uppsala, Sweden) for replacement of the buffer with 10 mM 4-(2-hydroxyethyl)-1-piperazineethanesulfonic acid (HEPES), pH 7.4.

For expression in mammalian cells, the indicator's ORF was subcloned into the pcDNA3.2 vector (Life Technologies). For organelle targeting, subcloning was performed into modified pcDNA3.2 vectors containing either the human ornithine transcarbamylase signal sequence (for mitochondrial targeting)[13] or the calreticulin signal sequence/KDEL motif [for endoplasmic reticulum (ER) targeting].

2.2 *Seminative Sodium Dodecyl Sulfate Polyacrylamide Gel Electrophoresis of Purified Protein Samples or HeLa Cells Lysate*

The purpose of seminative sodium dodecyl sulfate polyacrylamide gel electrophoresis (SDS PAGE) was to conduct the separation of the proteins contained in the sample, preserving, at the same time, the ability of FPs to emit light when excited. For this purpose, the procedure for SDS PAGE did not include the step of heat treatment of the sample to avoid the denaturation of all contained proteins. Seminative SDS PAGE was carried either for the purified protein sample of MagIC or for the lysate of HeLa cells expressing MagIC in the cytosol. The protein sample was prepared by dilution with sample buffer containing 2% SDS, 62.5 mM Tris–HCl (pH 6.8), 5% (v/v) β-mercaptoethanol, 10% glycerol (v/v) and bromophenol blue. The lysate of HeLa

expressing cytosolic MagIC was prepared as follows: cells grown on a 10-cm plastic plate 24 h after transfection (see Sec. 2.5) were washed with 4 mL ice cold PBS, and then detached by scrapping and resuspended in 2 mL ice-cold PBS for washing. After a centrifugation step (1000 × g, 10 min), the supernatant was removed and cells were resuspended in 100 μL of the sample buffer described above and applied directly to the polyacrylamide gel. The separation (a variant of this procedure is provided in Ref. 14) was performed using 12% separating polyacrylamide gel in the presence of 10% SDS.

2.3 *Spectral Characterization of the Mg^{2+}/Ca^{2+}-Sensitive Venus Fusion Constructions with Reference FPs*

For the indicator variants (containing different reference FPs), characterization of the Mg^{2+}-sensitivity of the absorption, excitation, and emission spectra was conducted. For this, protein samples diluted in 20 mM HEPES-KOH buffer (pH 7.2) were analyzed in a V-630 Bio spectrophotometer (JASCO; for absorption measurements), in a F-2500 fluorescence spectrophotometer (Hitachi, Japan; for excitation spectra acquisition) or in F7000 fluorescence spectrophotometer (Hitachi; for emission spectra acquisition) either in the absence or presence of 5 mM Mg^{2+}.

Absorption spectra were acquired in the 450 to 600 nm range.

Excitation spectra for each of the constructions were acquired separately for the Venus variant (monitored wavelength corresponding to its emission maximum, 530 nm) and the corresponding reference FP (monitored at the respective emission maximum of the reference FP). These monitored wavelengths were, specifically, 610 nm for mCherry, 633 nm for mKate2, 563 nm for mKOκ, and 565 nm for the nonphotoconverted PSmOrange. After these separate measurements (for Venus and the reference FP) were conducted in the absence of Mg^{2+}, 5 mM Mg^{2+} were added into the same cuvette and the measurements were repeated.

Similarly, emission measurements of the PSmOrange-[Mg^{2+}-sensitive cp173Venus], mKOκ-[Mg^{2+}-sensitive cp173Venus] and mKate2-[Mg^{2+}-sensitive cp173Venus] constructions were conducted. In this case, the Venus variant fluorescence and the emission of the reference FP were acquired using separate excitation. In all constructions, the Mg^{2+}-sensitive Venus was excited with 516-nm light (bandwidth 5 nm). Emissions of the corresponding reference FPs were obtained by excitation with the following wavelengths: 548 nm for PSmOrange, 551 nm for mKOκ, and 588 nm for mKate2. In detail, characterization of the Mg^{2+}-sensitivity of the emission spectrum of mCherry-[Mg^{2+}-sensitive cp173Venus] construction (MagIC) is provided in Sec. 2.4.

2.4 *In Vitro Analysis of MagIC*

Affinity and selectivity were determined by separate excitation of the Mg^{2+}/Ca^{2+}-sensitive Venus variant (excitation 516 nm) and mCherry (excitation 587 nm) in an F-7000 fluorescence spectrophotometer (Hitachi).

The indicator affinity was determined using serial dilutions of $MgCl_2$ in a background of 100 mM KCl and 10 mM MOPS (pH 7.4, KOH). Selectivity (as the ability to displace Mg^{2+} at physiological concentrations from the created binding site) was assayed in solutions with 100 mM KCl and 1 mM $MgCl_2$, 10 mM MOPS (50 mM for the case of polyamines) (pH 7.4) and the ion of interest and then compared with a similar solution without that ion. pH sensitivity of the indicator was analyzed in solutions containing either 10 mM MES–HEPES (pH range 5.5 to 8.0) or Tris (pH 8.3 to 9.0) in a background of 100 mM KCl and 1 mM $MgCl_2$.

2.5 *Cell Culture and Transfection*

HeLa cells were cultured at 37°C in Dulbecco's modified Eagle's medium (DMEM, Sigma) supplemented with 10% heat-inactivated fetal bovine serum (FBS, Biowest) in a 5% CO_2 atmosphere.

Pituitary cells of the GH3 line (ATCC CCL-82.1) were maintained in DMEM/F12 + GlutaMAX (Gibco, Life Technologies) supplemented with 2.5% FBS (Biowest) and 15% heat inactivated horse serum (Gibco, Life Technologies) in 5% CO_2 atmosphere.

Cell transfection was carried as in the "Ca^{2+}-phosphate" method[15] or with Lipofectamine 2000 (Life Technologies) following the manufacturer's protocol. Simultaneous expression of different indicators was achieved by cotransfection with a 1:1 mixture of plasmids containing the indicators.

2.6 *General Imaging Conditions*

Cell imaging was performed 24 to 48 h after transfection using a Nikon Ti Eclipse confocal microscope equipped with 60× oil immersion lens (NA: 1.4) and a Nikon A1 imaging system. Experiments, if not otherwise specified, were conducted at room temperature (around 25°C).

2.7 *Imaging with Indicators in Cells*

In the present work, three genetically encoded indicators were used: MagIC (or the negative control mCherry-cp173Venus), B-GECO1—a genetically encoded Ca^{2+} indicator [$K_d(Ca^{2+}) = 164$ nM],[16] and pHluorin—a genetically encoded pH indicator (pK_a around 7.0).[17]

In experiments with cells expressing MagIC or the negative control mCherry-cp173Venus, the Venus variants were excited with a 488-nm laser and their emissions were collected in the 500 to 550 nm range. mCherry excitation was performed with a 561 nm laser and its emission was collected in the 570 to 620 nm range. When MagIC was coexpressed with B-GECO1,[16] a genetically encoded Ca^{2+} indicator with excitation and emission maxima at 378 and 446 nm, respectively, this last was excited with a 403.5-nm laser, and emission was read in the 425 to 475 nm range. Channels were acquired sequentially.

Excitation of ratiometric pHluorin was performed with 403.5 and 488 nm lasers and the corresponding emissions were read in the 500 to 550 nm range.

2.8 *Image Analysis*

Image analysis was performed with ImageJ and Metamorph (Molecular Devices, United States). MagIC ratio images were obtained dividing the Venus channel by the mCherry one after background subtraction.

2.9 *In Situ Mg^{2+} Sensitivity*

Mg^{2+} sensitivity of the indicator expressed in cells was assayed as follows: cells expressing MagIC or mCherry–cpVenus, used as a negative control, were washed with Mg^{2+}/Ca^{2+}-free Hanks balanced salt solution [HBSS(−); Sigma, containing, in mM:

KCl, 5.33; KH_2PO_4, 0.44; NaCl, 138; $NaHCO_3$, 4.0; Na_2HPO_4, 0.3; glucose, 5.6; pH in the 7.2 to 7.6 range] and then the cellular membrane was permeabilized with 20 μg/mL digitonin in HBSS(−). To this, 10 mM Mg^{2+} in HBSS(−) was added, followed by the application of a saturating (20 mM) concentration of EDTA in HBSS(−).

2.10 *Hyperosmotic Shock of HeLa Cells*

HeLa cells cultured in glass-bottom dishes for 48 h after transfection were imaged in their original medium (DMEM + 10% FBS) at 5-s interval for 10 min at room temperature. Application of the hyperosmotic shock was performed by removing the cell medium and simultaneously, a new medium with either $MgCl_2$, KCl, or D-sorbitol (Wako Chemicals, Japan) was added to obtain the equimolar final concentrations of 50 mM $MgCl_2$, 75 mM KCl, or 150 mM D-sorbitol in the imaged dish.

3 Results

3.1 *Indicator Design*

Mg^{2+}-sensitivity of the indicator was achieved following a strategy similar to that one used for the development of the low affinity Ca^{2+} indicator CatchER.[12] In the present study, three of the five negatively charged residues (corresponding to 147E, 202D, and 204E in CatchER) were sequentially introduced into cp 173 Venus,[18,19] becoming 220E, 31D, and 33E, respectively (in cp173Venus numeration, Table 1). Additional spontaneous mutations G4S (EGFP 177S), V89I (EGFP 18V), and Q142M (EGFP 72Q) were found in the brightest colonies expressing the Mg^{2+}/Ca^{2+}-sensitive cpVenus variant. Of these, the last two were preserved in the final indicator construction. In addition, the following variants of the Mg^{2+}/Ca^{2+}-sensitive cp173Venus were created: (1) with the five negative residues of CatchER, (2) with the five negative residues and reversed spontaneous mutations, and (3) with the three negative residues and reversed spontaneous mutations. However, the resulting fluorescence of all these variants in bacterial cells was dimmer (not shown). The chosen indicator variant (corresponding to the brightest colonies) displayed a variation in the fluorescence intensity as a function of the applied Mg^{2+} or Ca^{2+} concentration and constituted the intensiometric (Mg^{2+}/Ca^{2+}-sensitive) part of the indicator.

Unlike other single-FP based indicators (e.g., Camgaroos,[20] Pericams,[21] GECOs,[16] or G-CaMPs[22,23]), in our case, the fluorescence intensity variation upon ion binding was not provoked by large intramolecular conformational changes (see details in Ref. 12). This feature led us to introduce a second FP as a constant reference, the fluorescence intensity of which did not depend on Mg^{2+} or Ca^{2+} levels, thus allowing ratiometric imaging of changes in the concentration of these ions [Fig. 1(a)]. The resulting indicator required irradiation at two separate wavelengths: one to obtain the intensiometric signal from the Mg^{2+}/Ca^{2+}-sensitive Venus variant, and the other to obtain the reference signal used to perform the signals' ratioing.

3.2 *Selection of the Reference FP*

To avoid undesirable resonance energy transfer between the two proteins in the indicator, FPs with excitation peaks at wavelengths longer than the emission maximum of the Mg^{2+}/Ca^{2+}-sensitive Venus variant (530 nm) were selected as reference. As mentioned above, the reference fluorescence intensity should by itself be insensitive to variations in Mg^{2+}/Ca^{2+} concentrations. In addition to this requirement, the reference fluorescence intensity should be large enough to reduce errors related to the stochastic character of the photon emission process, which can result in errors in the final ratio image.

Table 2 Fluorescent proteins (FPs) tested as reference to obtain a ratiometric low affinity Mg^{2+}/Ca^{2+}-sensitive indicator.

FP	Excitation/emission wavelengths, nm	References
PSmOrange	548/565|636/662	25
mKOκ	551/563	26
mCherry	587/610	24
mKate2	588/633	27

From the tested FPs (Table 2), the closest one to meet all the above requirements was mCherry.[24] An initial approach to use photoconverted PSmOrange (excitation/emission maxima 636/662 nm)[25] resulted in almost complete absence of the Venus fluorescence due to photobleaching by the intense 475/28 nm light used for photoconversion, without significant changes observed in the optical properties of PSmOrange (not shown). On the other hand, the nonphotoconverted PSmOrange (excitation/emission maxima 548/565 nm) proved the viability of the chosen approach for *in vitro* ratiometric imaging using a reference fluorescence signal. PSmOrange emission did not interfere with the Mg^{2+}/Ca^{2+}-sensitive Venus fluorescence and could be detected separately, though this result is impractical for imaging due to low fluorescence intensity [Fig. 2(c)] and requirement of somewhat complicated filter sets in the microscopy system. In the case of other reference FPs, mKOκ,[26] and mKate2,[27] either Venus fluorescence was lost due to almost complete FRET [mKOκ; Fig. 2(c)] or the reference fluorescence was too dim [mKate2; Fig. 2(c)]. Moreover, the analysis of the excitation, absorption and emission spectra of PSmOrange, mKOκ, and mKate2 (in fusions with Mg^{2+}-sensitive cpVenus) revealed their sensitivity to addition of 5 mM Mg^{2+} (Fig. 2) and only mCherry spectra remained unchanged. Thus, we confirmed that mCherry fluorescence intensity is stable enough to serve as a constant reference for the indicator.

The fusion of mCherry with the Mg^{2+}/Ca^{2+}-sensitive moiety described in Sec. 3.1 constituted the final indicator, termed as MagIC [Fig. 1(b)].

We should mention that during our work we found that the non-FRET ratiometric imaging approach referred to here has already been applied in several previous studies,[28,29] which also used mCherry as a reference FP. In these studies, however, the performance of other reference FPs was not analyzed.

3.3 In Vitro *Properties of MagIC*

As the reported Mg^{2+} concentration in MagIC relies on the ratio of fluorescence signals from two FPs, a preferential expression of one of them could potentially alter the results of measurements. That is why after purification, the protein samples were tested by seminative SDS PAGE to estimate their purity and the indicator integrity. For this purpose, the samples with SDS were subjected to PAGE without preliminary heating. Under these conditions, FPs retain their fluorescence and can be easily visualized on excitation using appropriate light. Our results show that more than 90% of the observed fluorescent

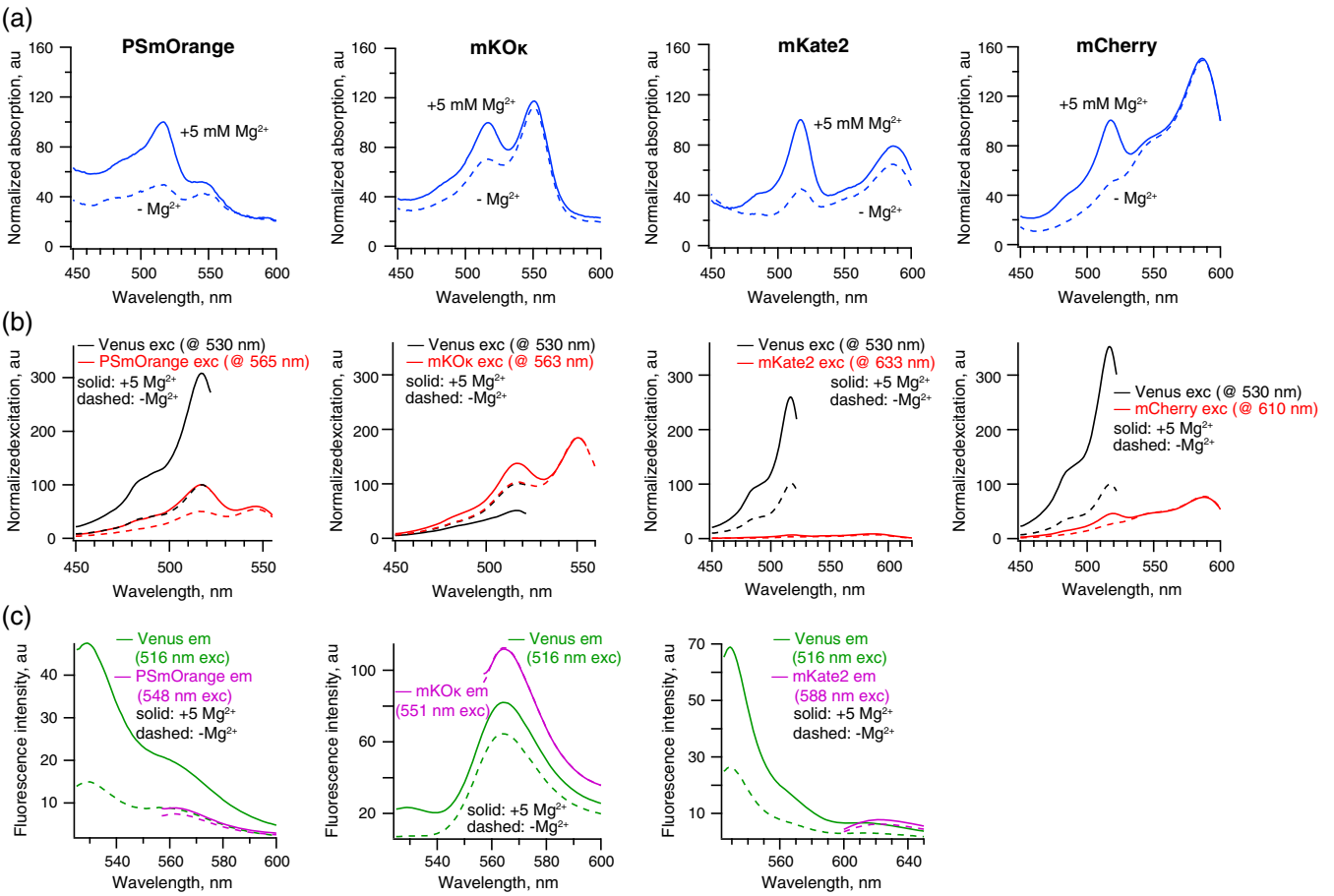

Fig. 2 Selection of an appropriate Mg^{2+}-insensitive reference fluorescent protein (FP). Shown are absorption, excitation, and emission spectra of the reference FPs (in fusion with the Mg^{2+}/Ca^{2+}-sensitive Venus variant) in absence (dashed lines) or presence (solid lines) of Mg^{2+} (5 mM). (a) Absorption spectra (blue lines) of constructions normalized to Mg^{2+}-sensitive Venus absorption peak at 516 nm in the presence of 5 mM Mg^{2+}. The right peak in the spectra corresponds to the absorption maximum of the specified reference FP. Only the mCherry absorption peak remains unchanged after addition of 5 mM Mg^{2+}. (b) Excitation spectra of the constructions normalized to the excitation maxima of the Mg^{2+}-sensitive Venus in absence of Mg^{2+}. The excitation of the Mg^{2+}/Ca^{2+}-sensitive Venus in all constructions (black lines) was monitored at its emission maximum (530 nm). The monitored wavelengths for the reference FPs (in red lines) were—PSmOrange, 565 nm; mKOκ, 563 nm; mKate2, 633 nm; mCherry, 610 nm—as displayed in the corresponding legends. As in the case of absorption spectrum, the excitation peak of mCherry is unaffected by Mg^{2+} addition. Note the decrease of the excitation peak of mKOκ after Mg^{2+} addition due to FRET from the Venus variant to mKOκ. (c) Emission spectra obtained by separate excitation of either the Mg^{2+}-sensitive Venus variant (green lines) or the reference FP (magenta lines) within the fusion constructions. Emission of the Venus variant in all cases was obtained by excitation with 516-nm light. The excitation wavelengths for the references were—548 nm, for PSmOrange; 551 nm, for mKOκ; 588 nm, for mKate2. Note the almost complete absence of the Venus emission peak in the mKOκ-[Mg^{2+}-sensitive cp173Venus] construction due to FRET. Traces are the average of three independent measurements.

band intensity corresponds to the correct construction in the purified protein sample [Fig. 3(a)].

First, we tested *in vitro* the affinity of our indicator to Mg^{2+}. The emission spectrum of MagIC displays a rising 610-nm peak with an increase in the applied Mg^{2+} concentration when the Mg^{2+}/Ca^{2+} sensitive Venus variant is excited [Fig. 3(b)]. The intensity of this peak is higher than the intensity of separately excited mCherry, suggesting that it is provoked both by excitation of mCherry and the emission of the Venus variant at wavelengths longer than 580 nm. Such undesired FRET forced us to acquire the reference signal by a separate excitation, not only *in vitro* but also during imaging.

To determine the indicator affinity for Mg^{2+}, solutions with Mg^{2+} concentrations ranging from 0 to 25 mM were used. The calculated affinity constant for this ion in the presence of 100 mM KCl at room temperature was $K_d(Mg^{2+}) = 5.1$ mM (Hill constant $n = 1.1$) [Fig. 3(d)] with saturation around 20 mM Mg^{2+}.

The designed Mg^{2+}-chelating site does not exclude the possibility of other divalent cations binding, so the selectivity of MagIC for several of these cations was tested. As shown in Fig. 3(c), the indicator also displays affinity for Ca^{2+} in the millimolar range [$K_d(Ca^{2+}) = 4.8$ mM, $n = 0.8$]. This suggests that, similar to many other fluorescent dyes used for cytosolic

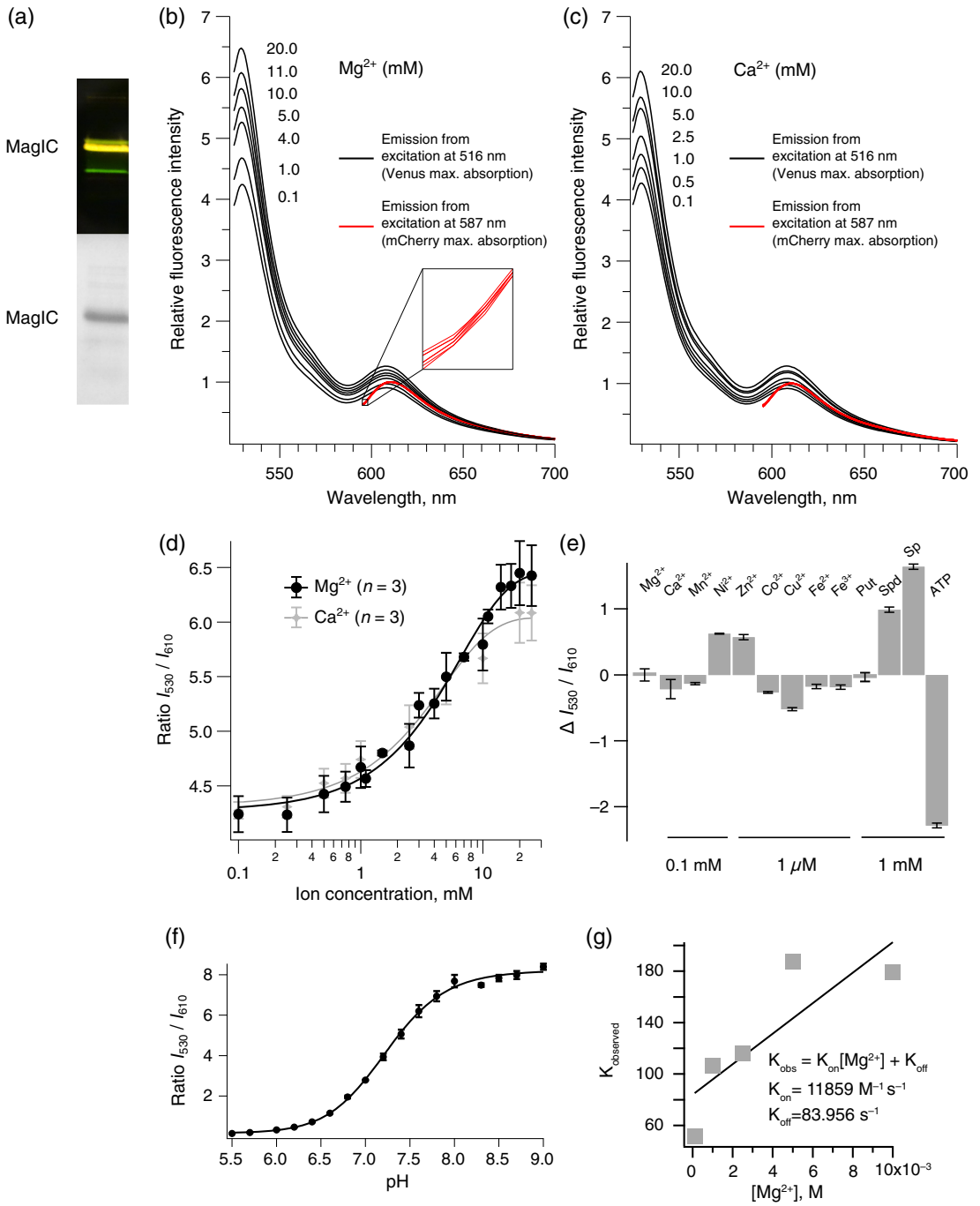

Fig. 3 *In vitro* properties of MagIC. (a) Seminative SDS PAGE of a purified sample of MagIC; fluorescence acquired with a conventional digital camera through an orange filter (top) and gel stained with Coomassie Brilliant Blue (bottom). (b) and (c) Emission spectra of MagIC as a function of the applied concentrations of divalent cations. Following the principle shown in Fig. 1, the fluorescence intensity of the Mg^{2+}/Ca^{2+}-sensitive Venus variant increases with an increasing concentration of either Mg^{2+} [in (b)] or Ca^{2+} [in (c)]. The fluorescence spectra of mCherry (in red), taken separately, are not affected by addition of either Mg^{2+} or Ca^{2+}. The zoomed inset in (b) shows a fragment of the mCherry spectra obtained at the different tested Mg^{2+} concentrations. (d) Calibration curve obtained by ratioing the fluorescence intensities of the two components of the indicator, obtained at room temperature (25°C). The dynamic range of the indicator is 1.5. (e) Selectivity of MagIC is shown as the change in the ratio induced by the application of inorganic cations, polyamines or ATP in 1 mM Mg^{2+} background. Respective ions or compounds were added at the specified concentrations and then the ratio difference was calculated by subtracting the ratio at 1 mM Mg^{2+}. The 530/610 ratio at 1 mM Mg^{2+} is 4.7 (25°C). Put, putrescine; Spd, spermidine; Sp, spermine. (f) pH dependency of the (I_{530}/I_{610}) ratio in a background of 100 mM KCl and 1 mM $MgCl_2$. The pK_a of the indicator determined under these conditions is 7.5. (g) Relaxation constant $k_{obs}([Mg^{2+}])$ for MagIC as a function of the applied Mg^{2+} concentration. Rate constants, k_{on} and k_{off}, were determined by fitting the equation $k_{obs} = k_{on}[Ca^{2+}] + k_{off}$. Their values at 31°C are presented.

Mg^{2+} monitoring, our indicator is also a low affinity (though of millimolar order) Ca^{2+} indicator.

The selectivity of MagIC in 1 mM Mg^{2+} was analyzed against Ca^{2+}, Mn^{2+} or Ni^{2+} at a concentration of 0.1 mM each. In the presence of these concentrations, much larger than their normal levels in the eukaryotic cell cytosol, the (Venus/mCherry) ratio of MagIC remained almost unaffected. Co^{2+}, Cu^{2+}, Fe^{2+}, and Fe^{3+} at micromolar concentrations also did not show any noticeable effect on the ratio value observed for Mg^{2+} alone [Fig. 3(e)]. The ratio value, however, was increased by the application of 1 mM spermine and spermidine, polyamines, which are known to compete with Mg^{2+} for binding sites in nucleic acids [Fig. 3(e)]. Interestingly, application of 1 mM ATP provoked a strong decrease in the (Venus/mCherry) ratio, indicating competition with MagIC for Mg^{2+} by this high affinity Mg^{2+} chelator [$K_d(Mg^{2+}) = 50\ \mu M$],[30] suggesting at the same time that our indicator does not sense Mg-ATP. The pKa of MagIC, as in the case of CatchER,[12] the pKa of MagIC is 7.5 [Fig. 3(f)], being the Mg^{2+}/Ca^{2+}-sensitive Venus the main pH-sensitive component. Analysis of the kinetics of Mg^{2+}-binding by MagIC using the stopped flow method revealed values of $k_{on} = 11859\,M^{-1}s^{-1}$ and $k_{off} = 83.956\ s^{-1}$ [at 31°C; Fig. 3(g)].

3.4 *MagIC can be Selectively Targeted to Different Intracellular Compartments*

MagIC is a genetically encoded indicator; so, in a next step, we analyzed its intracellular distribution when expressed in cells and the possibility of its targeting to specific intracellular locations. Expression of MagIC in HeLa cells without any particular targeting sequence resulted in mixed cytosolic and nuclear localization, a unique feature of our Mg^{2+} indicator [Fig. 4(a)]. MagIC-transfected cells were easily identified both by the bright yellow–green fluorescence of Mg^{2+}/Ca^{2+}-sensitive Venus and by the red fluorescence of mCherry.

Expression of MagIC in fusion with the targeting sequence of human ornithine transcarbamylase resulted in mitochondrial localization of the sensor [Fig. 4(a)], being it's both components highly fluorescent at this organelle. On the other hand, MagIC targeted to ER displayed significantly reduced fluorescence of the Mg^{2+}/Ca^{2+}-sensitive Venus [Fig. 4(a)]. This effect was not indicative of low level of divalent cations in the ER, as the ER-targeted negative control mCherry–cpVenus displayed even lower yellow–green fluorescence when imaged under similar conditions (not shown).

A seminative SDS PAGE of the nonboiled lysate of HeLa cells expressing cytosolic MagIC displayed a single fluorescent band, indicating the expression of FPs predominantly within the full indicator construction [Fig. 4(b)].

3.5 *In Situ Mg^{2+} Sensitivity and Calibration of MagIC*

Having determined the *in vitro* properties of MagIC, we next analyzed its Mg^{2+}-sensitivity in cells. For this purpose, we initially incubated cells in solutions with increasing Mg^{2+} concentrations in the presence of ionomycin—a divalent cation ionophore. Under these conditions, MagIC displayed an increasing ratio with the increase in the extracellular Mg^{2+} concentration. However, in each case, the equilibration of the system took a relatively long time, during which the cell shape was altered, probably as a response to cytosolic Mg^{2+} elevation (not shown).

In addition to these difficulties, we also found concerns in the literature regarding the use of ionophores to equilibrate Mg^{2+} concentration in cells (see in Ref. 5). To overcome this, we decided to analyze the in-cell Mg^{2+} sensitivity of MagIC using a different strategy. In the new scheme, HeLa cells expressing MagIC were treated with 20 $\mu g/mL$ digitonin at the beginning of the experiment to permeabilize the cell membrane. Next, 10 mM Mg^{2+} was applied followed by the application of 20 mM EDTA. In these conditions, MagIC reported an increase in the (Venus/mCherry) ratio when Mg^{2+} was added and showed a pronounced decrease in the ratio value upon EDTA addition [Figs. 4(c) and 4(d)]. At the same time, no change in the (Venus/mCherry) ratio value was observed in the case of cells expressing mCherry–cpVenus, which was used as a negative control [Fig. 4(e)], indicating that the ratio changes observed in the case of MagIC corresponding to changes in the free Mg^{2+} concentration.

3.6 *MagIC is Insensitive to Cytosolic Ca^{2+} Elevations*

As MagIC shows sensitivity to Ca^{2+} (though in the millimolar range), we next tested the possibility that its ratio value could be affected by elevations in the cytosolic Ca^{2+} levels. For this purpose, we coexpressed MagIC with the genetically encoded Ca^{2+} indicator B-GECO1[16] in pituitary cells, which are known to generate spontaneous Ca^{2+} transients. Simultaneous monitoring of cytosolic Mg^{2+} and Ca^{2+} dynamics in this cell line at 37°C in DMEM-F12 first showed that MagIC is insensitive to the cytosolic Ca^{2+} increase and indicated at the same time that the cytosolic Mg^{2+} dynamics was not affected by the generation of these Ca^{2+} spikes, at least during the course of imaging [Figs. 4(f) and 4(g)].

3.7 *Hyperosmotic Shock Induces MagIC Ratio Increase in HeLa Cells*

With the experiments presented above, we could confirm the Mg^{2+} sensitivity of MagIC expressed in cells, however, the most demanding part of the work was to search for an appropriate stimulus that could induce visible changes in the cytosolic Mg^{2+} level. This task was further hindered by the fact that cytosolic free Mg^{2+} concentration seems to be tightly regulated even in situations when the stimulus induces a large Mg^{2+} flux through the plasma membrane.[6]

We initially focused on nordihydroguaretic acid (NDGA) a polyphenolic compound abundant in the creosote bush (*Larrea tridentata*), and which was reported to enhance the Na^+-dependent Mg^{2+} efflux mediated by the plasma membrane-located Na^+/Mg^{2+} exchanger,[31] and is, in addition, a potent inhibitor of the TRPM7—one of the main cellular Mg^{2+}-uptake systems.[32] Application of NDGA (50 μM) to cells expressing MagIC provoked an immediate and strong decrease in the (Venus/mCherry) ratio that achieved its minimum within 5 min and was thereafter maintained constant at this low level during the course of imaging [Figs. 5(a) and 5(b)]. It appeared, however, that acidification of the cytosol was largely responsible for this effect, as the negative control mCherry–cpVenus also displayed a (Venus/mCherry) ratio decrease with a very similar time course [Figs. 5(c) and (d)]. Interestingly, simultaneous application of NDGA (enhancer of Na^+/Mg^{2+} exchange)[31] and 100 μM imipramine (inhibitor of the corresponding exchanger)[31,33] slightly delayed the onset of the MagIC ratio

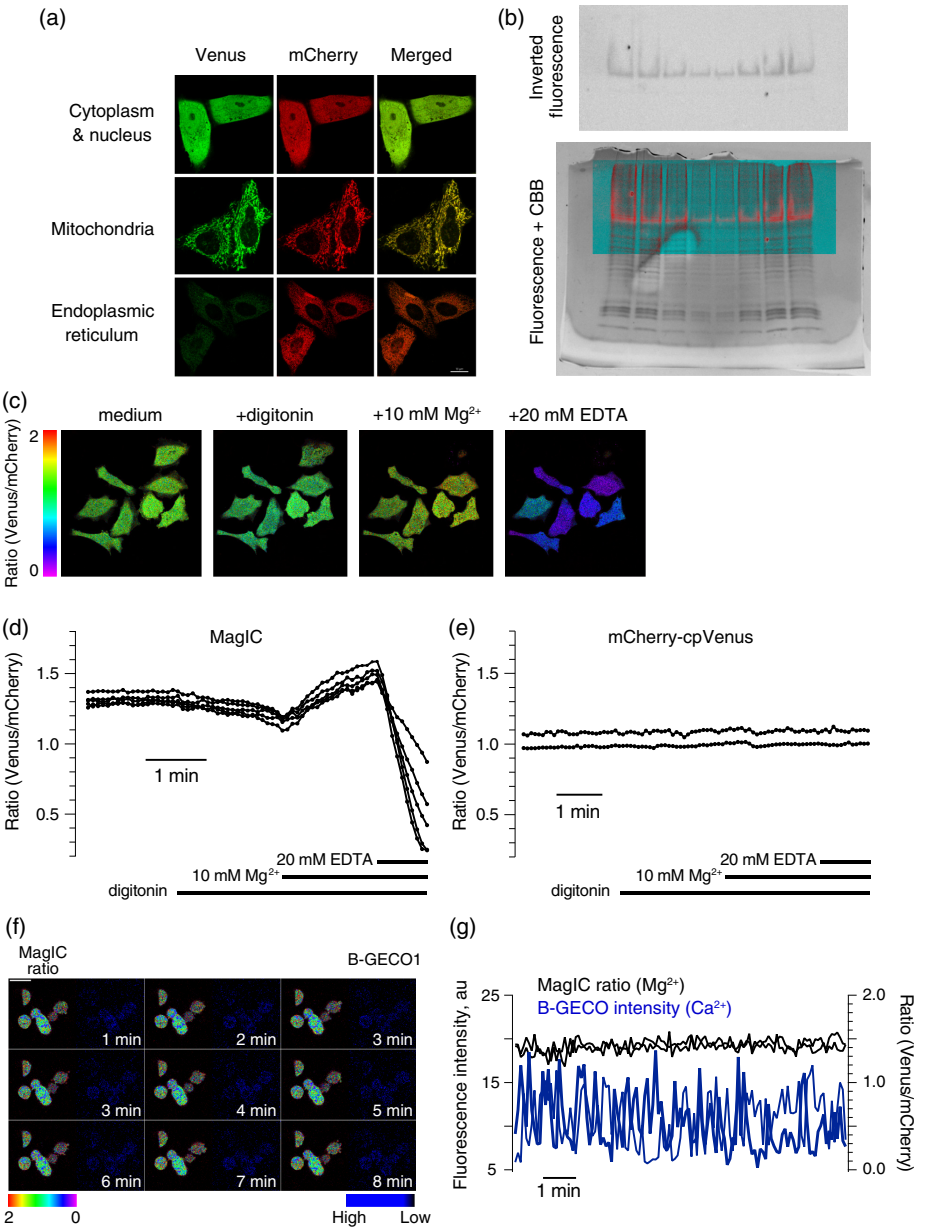

Fig. 4 *In situ* properties of MagIC. (a) Expression pattern of MagIC in HeLa cells without targeting sequences (top; cytosolic and nuclear localization), targeted to mitochondria (middle) and to the endoplasmic reticulum (bottom). (b) Seminative SDS PAGE of nonheated lysate of HeLa cells expressing cytosolic MagIC. A single fluorescent band is observed (top), corresponding to the indicator. At the bottom is shown the overlay of the fluorescence image with other cellular proteins stained with Coomassie Brilliant Blue (CBB). In (c) and (d), Mg^{2+} sensitivity of MagIC was assayed with Mg^{2+}/EDTA in digitonin-permeabilized HeLa cells. Experiments were conducted at 21°C. (c) (Venus/mCherry) ratio images in each of the applied conditions. (d) Time course of the change in the ratio in cells from (c). (e) The negative control mCherry–cpVenus does not show Mg^{2+}-dependent ratio changes. (f) and (g) MagIC is insensitive to cytosolic Ca^{2+} increase. MagIC was coexpressed with the Ca^{2+} indicator B-GECO1 in pituitary cells, in which spontaneous Ca^{2+} spikes are observed which do not provoke visible associated changes in the cytosolic Mg^{2+}. Imaging carried out at 37°C in Dulbecco's modified Eagle's medium-F12. (f) Representative images of the MagIC ratio (proportional to cytosolic Mg^{2+}) and the corresponding B-GECO1 fluorescence intensity (proportional to cytosolic Ca^{2+}) taken with 1 min interval. Corresponding images taken with 5-s interval during 10 min are shown in Video 1. The movie shows the calculated (Venus/mCherry) ratio for MagIC and the B-GECO1 fluorescence intensity for a representative group of cells. Color bars show the corresponding lookup tables (LUTs) for both images. (Venus/mCherry) ratio LUT range is 0 (violet) to 2 (red). For B-GECO1's channel LUT, the black color corresponds to low fluorescence intensity, and the light blue in the opposite extreme—to a higher fluorescence intensity. (g) Traces of MagIC ratio and B-GECO1 fluorescence intensity for representative cells shown in (f). Shown are representative experiments from 3 (Mg^{2+}-calibration) or 6 (Ca^{2+}/Mg^{2+} monitoring in GH3 cells) trials. Scale bars, 10 μm. Video 1 (MOV, 6.96 MB) [URL: http://dx.doi.org/10.1117/1.JBO.20.10.101203.1].

value decrease and reduced it, then finally induced the formation of large membrane blebs within a few minutes of application [Fig. 5(e)]—an effect which was not observed when either of these chemicals was applied alone [Fig. 5(f)].

In Ref. 10, the authors noted that their genetically encoded Mg^{2+} indicator, MagFRET, did not report $[Mg^{2+}]_{cyt}$ changes under several conditions which were previously reported to provoke $[Mg^{2+}]_{cyt}$ increase. These conditions were (as cited in Ref. 10): (1) application of elevated Mg^{2+} in the medium,[34] (2) application of Li^+ as Mg^{2+}-competitor,[35] and (3) perfusion with solutions containing variable Na^+ concentration,[36,37] each applied to different cell types. We decided to analyze which kind

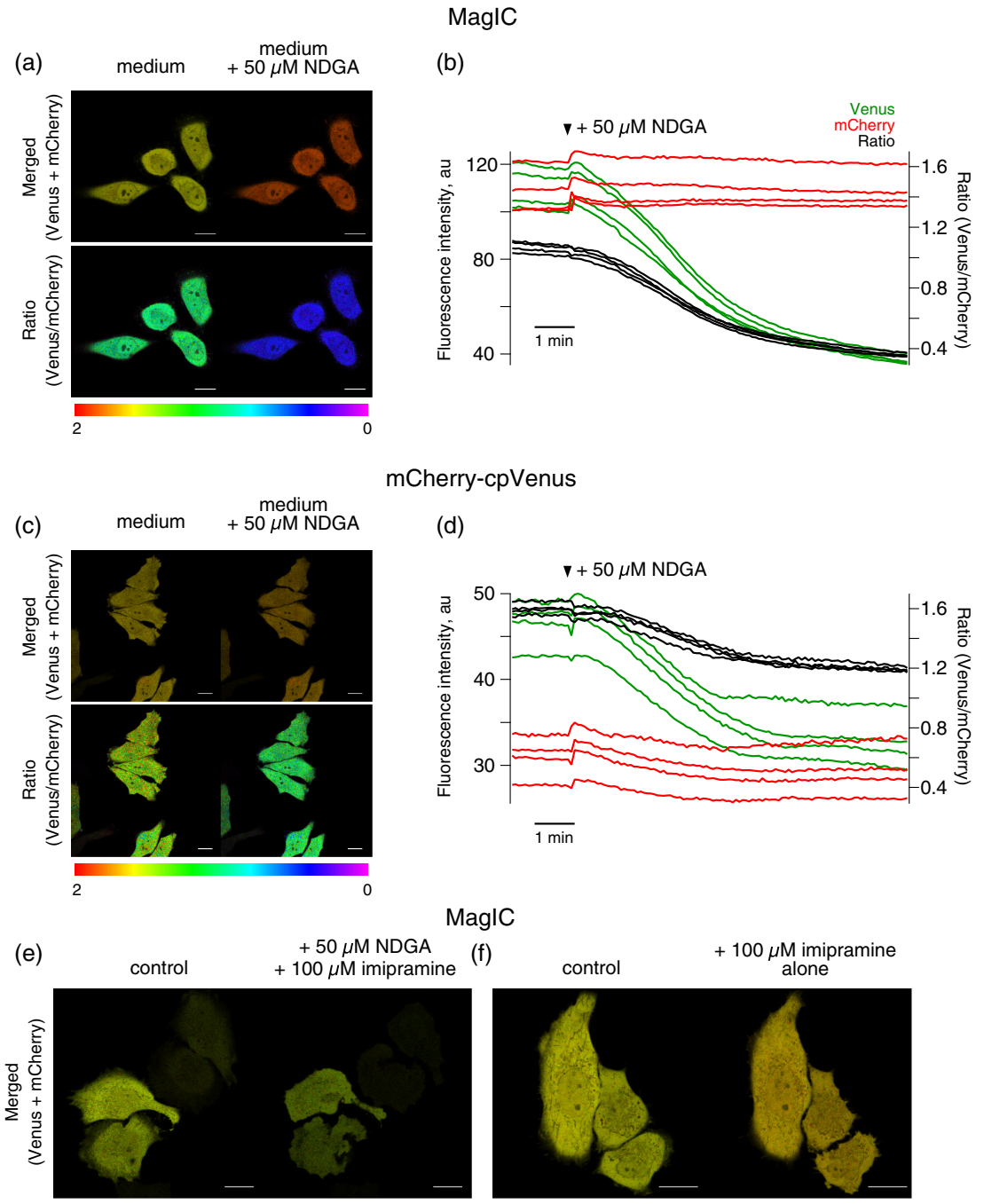

Fig. 5 Effect of nordihydroguaretic acid (NDGA) application on the (Venus/mCherry) ratio of MagIC expressed in HeLa cells. (a and b) Effect of NDGA alone on the ratio value of MagIC expressed in HeLa cells. Application of NDGA in HBSS(–) induced an almost immediate decrease of the (Venus/mCherry) ratio. (a, top) Merged (Venus + mCherry) images of cells before (left) or after (right) application of 50 μM NDGA. (a, bottom) Pseudocolored images of the same cells displaying the ratio change induced by NDGA application. (b) Time courses of the ratio decrease for the cells shown in (a). (c and d) The negative control, mCherry–cpVenus displays a similar (Venus/mCherry) ratio decrease, suggesting that this effect is produced by the cytosol acidification. (e and f) Addition of NDGA together with the inhibitor of the Na^+/Mg^{2+} exchanger imipramine (100 μM) induces blebs formation (e, right), an effect which is not observed when imipramine is added alone (f). Scale bars, 10 μm.

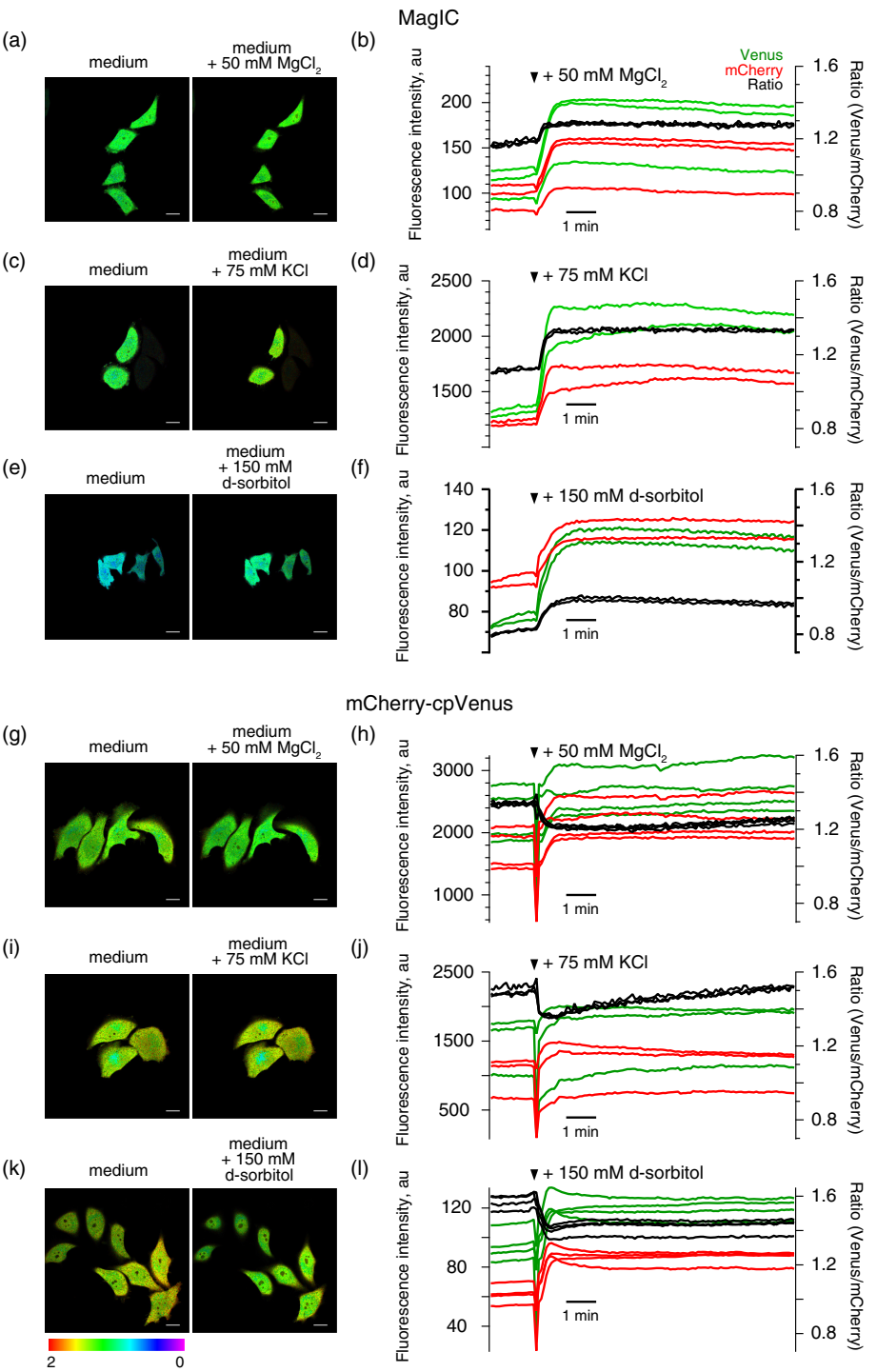

Fig. 6 Hyperosmotic shock induces cytosolic MagIC ratio increase. HeLa cells expressing either MagIC. (a–f) or mCherry–cpVenus (g–l) were treated with either 50 mM $MgCl_2$, 75 mM KCl, or 150 mM D-sorbitol applied to the original medium. (a) and (b) Similar to results reported in previous studies,[34] 50 mM $MgCl_2$ stimulation induces an apparent cytosolic Mg^{2+} increase which is reported by MagIC. However, application of an equimolar amount of KCl (c and d) or D-sorbitol (e and f) in the medium induces a similar apparent Mg^{2+} increase, suggesting that it is provoked by the resulting high osmotic potential of the medium, and not by the extracellular Mg^{2+} itself. Part of this response, however, seems to be associated to nonspecific changes in the intracellular milieu provoked by hyperosmotic stresses, as ratio changes were also observed in the ratio reported by the Mg^{2+}-insensitive negative control mCherry–cpVenus (g–l). Application of hyperosmotic media (with either $MgCl_2$, KCl or D-sorbitol) in this case also induce (Venus/mCherry) ratio changes, though oppositely directed to those reported by MagIC. Shown are images of cells in the medium before (left) and after the addition of the indicated osmolyte (right). Traces correspond to the measured intensities of the Venus variants (green) and mCherry (red) fluorescence intensities, and the calculated (Venus/mCherry) ratios for the shown cells. Experiments were repeated at least three times under each condition. Scale bars, 10 μm.

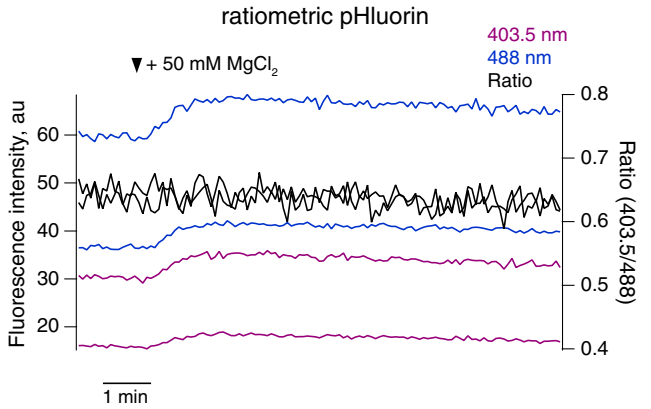

Fig. 7 Hyperosmotic shock does not affect cytosolic pH. HeLa cells expressing ratiometric pHluorin in the cytosol were stimulated by medium supplemented with 50 mM $MgCl_2$, as in a similar experiment in cells expressing MagIC [Figs. 6(a) and 6(b)]. The emissions produced by excitation with either 403.5 or 488 nm lights display an increase in fluorescence intensity similar to that observed for the Mg^{2+}-sensitive cp173Venus and mCherry in MagIC. However, the (403.5/488) ratio value does not show evidence of cytosolic pH change induced by this stimulation.

of response is reproduced in HeLa cells expressing MagIC in one of these conditions, namely, stimulation with high extracellular Mg^{2+}.

In our experiments, treatment of HeLa cells expressing MagIC with 50 mM $MgCl_2$ induced a significant MagIC ratio increase [Figs. 6(a) and 6(b)]. This result is similar to that previously observed with the Mg^{2+}-selective dye KMG-104 in HEK293T cells.[34] The applied Mg^{2+} concentration (50 mM) is, however, significantly higher than the Mg^{2+} level present in physiological fluids (around 1 mM, reported elsewhere) and provoked visible shrinking of the treated cells. So, to analyze whether the MagIC ratio increase was a specific response to the high extracellular Mg^{2+} or to the associated hyperosmotic shock, we replaced $MgCl_2$ by an equimolar amount of KCl or the carbohydrate D-sorbitol. Application to cells of either 75 mM KCl [Figs. 6(c) and 6(d)] or 150 mM D-sorbitol [Figs. 6(e) and 6(f)] in the medium induced a MagIC ratio increase similar to that provoked by the elevated extracellular Mg^{2+}, indicating that the presence of this last response is not indispensable for the observed effect. Part of this response seems, however, to depend on a highly probable change in the cytosolic ionic strength due to cellular water loss, since the application of these osmolytes to cells expressing the negative control mCherry–cpVenus also induced a slight (Venus/mCherry) ratio change, though in the opposite direction [Figs. 6(g)–6(m)].

To confirm that the changes observed with MagIC or the negative control mCherry–cpVenus were not associated to changes in the cytosolic pH, to which MagIC should be sensitive according to the measurements presented above [Fig. 3(f)], we performed monitoring of the cytosolic pH using a genetically encoded pH indicator, ratiometric pHluorin.[17] This indicator has two absorption maxima around 410 and 470 nm and a single emission peak. The (410/470) emission ratio of pHluorin is directly proportional to the pH in its environment, so we used it for monitoring cytosolic pH under hyperosmotic stimulation (Fig. 7). We performed imaging of cells expressing pHluorin with excitation by 403.5 and 488 nm lasers lines. In this case, addition to cells of medium supplemented with 50 mM $MgCl_2$ did not induce obvious changes in the cytosolic pH, indicating that the (Venus/mCherry) ratio increase reported by MagIC has a different origin.

4 Discussion

In contrast to Ca^{2+}, whose concentration in the cell cytosol is maintained low around hundredths of nanomoles, Mg^{2+} concentration is kept relatively high in the submillimolar to low millimolar range. The concentration change in the cell cytosol during physiological processes is also different for these ions: free Ca^{2+} concentration can rapidly increase at least 10 times, while free cytosolic Mg^{2+} level is generally considered less prone to significant variations.[6] Such differences in the behaviors of these ions should also influence the conditional differences in the response of their respective indicators: if for Ca^{2+} indicators a low basal fluorescence in resting conditions is desirable, such a property is difficult to achieve in Mg^{2+}-sensitive indicators of the appropriate affinity, which should be able to report small Mg^{2+} changes in the background of a relatively high concentration of this ion in the cell. Thus, contrary to Ca^{2+}, in resting conditions, a Mg^{2+} indicator with an appropriate affinity will necessarily show a nonzero signal, the intensity of which will depend on the Mg^{2+} concentration in its environment. Based on this assumption, we selected our indicator as the brightest probe from those expressed in bacterial cells. *In vitro* characterization of the chosen indicator, termed MagIC, proved its ability to change fluorescence properties upon Mg^{2+} increase from submillimolar concentrations up to 20 mM with a resulting relatively high dynamic range [Figs. 3(b) and 3(d)].

In FRET-based genetically encoded indicators, the signals from both FPs—the donor and acceptor—are detected simultaneously. This condition allows the monitoring of relatively fast Ca^{2+} spikes with a time resolution that depends mainly on the kinetic properties of the indicator. Free-cytosolic Mg^{2+} is also known to change under specific conditions, though this process takes several minutes,[6] so we considered that the time gap between the separate acquisition of the Mg^{2+}-sensitive channel and the reference is much shorter than the occurring changes in Mg^{2+} concentrations and will not drastically affect the measurement results. The kinetic properties of MagIC [Fig. 3(g)] also correspond to those of a relatively fast indicator; its dissociation constant k_{off} is around 84 s^{-1} [Fig. 3(g)], approaching those of fast organic indicators with k_{off} values in the 100 to 370 s^{-1} range.[38,39] However, the requirement of separate acquisition of both channels can potentially be a source of artifacts if the time between the acquisition of each channel is relatively long (for example, in the case of large images, slow scanning rates or fast-moving objects) and should also make the result undesirably sensitive to the mutual fluctuation of the excitation lights when separate light sources are used to obtain the signal from each of the MagIC's components.

The affinity of MagIC for Mg^{2+} is comparable to that of certain currently available Mg^{2+}-sensitive dyes [i.e., Mag-Fluo-4 with a $K_d(Mg^{2+}) = 4.7$ mM] with the advantage of millimolar-order affinity for Ca^{2+} [Figs. 3(c) and 3(d)] that should reduce the undesirable effects provoked by cytosolic Ca^{2+} increase, which is known to be able to affect measurements with conventional Mg^{2+}-sensitive dyes.[40] Indeed, in experiments with cells capable of generating spontaneous Ca^{2+} transients, we did not observe MagIC ratio changes that could suggest an interference from cytosolic Ca^{2+} [Figs. 4(f) and 4(g)]. On the other hand, even in an object with such unusual properties,

we could not find evidence of what could be a possible Mg^{2+} wave.

Finally, we cannot dismiss the possibility that the low-selectivity binding site of MagIC could make our indicator sensitive to intracellular species other than cytosolic Mg^{2+}. Particularly, as we have shown *in vitro*, intracellular polyamines could confound the results reported by our sensor [Fig. 3(e)]. Unfortunately, in the present study, we did not have the opportunity to corroborate our results with other available techniques of Mg^{2+} monitoring, however, our results are in good agreement with the results of previous studies (e.g., Ref. 33). We, nevertheless, have shown that the cytosolic Mg^{2+} increase, reported in Ref. 33 to be induced by high-extracellular Mg^{2+} treatment, is provoked by the high osmolality of the medium rather than by Mg^{2+} itself (Fig. 6).

MagIC, similarly to its prototype CatchER,[12] has a relatively high sensitivity to pH [pK_a = 7.5, Fig. 3(f)]. This sensitivity is probably not a big issue if Mg^{2+} monitoring is performed in the cytosol, as the pH in this compartment is rather stable[41] and close to the pK_a value of MagIC. However, if measurements with our indicator are to be performed in compartments or under conditions which are supposed to affect local pH, simultaneous monitoring of this parameter could allow distinguishing pH-related effects reported by MagIC from those induced by surrounding Mg^{2+} changes. There is an available plethora of fluorescent pH indicators, either organic dyes or genetically encoded pH-sensitive proteins, which can be used to test whether a specific experimental condition induces pH changes in the monitored compartment.

In conclusion, we validated the functionality of MagIC, a genetically encoded Mg^{2+} indicator based on a straightforward "modular" reporting mechanism, and we hope that it will serve as a useful tool for Mg^{2+} monitoring in different cellular compartments.

Acknowledgments

This work was supported by the Grant-in-aid for Scientific Research on Innovative Areas, 'Spying minority in biological phenomena (No. 3306)' from the Ministry of Education, Culture, Sports, Science and Technology, Japan (MEXT) (No. 23115003) to T. N.

References

1. A. M. P. Romani and A. Scarpa, "Regulation of cellular magnesium," *Front. Biosci.* **5**, d720–734 (2000).
2. Z. Grabarek, "Insights into modulation of calcium signaling by magnesium in calmodulin, troponin C and related EF-hand proteins," *Biochim. Biophys. Acta* **1813**(5), 913–921 (2011).
3. F. Y. Li et al., "Second messenger role for Mg^{2+} revealed by human T-cell immunodeficiency," *Nature* **475**, 471–476 (2011).
4. A. M. P. Romani, "Magnesium homeostasis in mammalian cells," *Front. Biosci.* **12**, 308–311 (2007).
5. R. D. Grubbs, "Intracellular magnesium and magnesium buffering," *BioMetals* **15**, 251–259 (2002).
6. A. M. P. Romani, "Cellular magnesium homeostasis," *Arch. Biochem. Biophys.* **512**, 11–23 (2011).
7. V. Trapani et al., "Intracellular magnesium detection: imaging a brighter future," *Analyst* **135**, 1855–1866 (2010).
8. B. Raju et al., "A fluorescent indicator for measuring cytosolic free magnesium," *Am. J. Physiol.* **256**(3), C540–C548 (1989).
9. H. Komatsu et al., "Design and synthesis of highly sensitive and selective fluorescein-derived magnesium fluorescent probes and application to intracellular 3D Mg^{2+} imaging," *J. Am. Chem. Soc.* **126**, 16353–16360 (2004).
10. L. Lindenburg et al., "MagFRET: The first genetically encoded fluorescent Mg^{2+} sensor," *PLoS One* **8**(12), e82009 (2013).
11. A. Sawano and A. Miyawaki, "Directed evolution of green fluorescent protein by a new versatile PCR strategy for site-directed and semi-random mutagenesis," *Nucl. Acids Res.* **28**(16), e78 (2000).
12. S. Tang et al., "Design and application of a class of sensors to monitor Ca^{2+} dynamics in high Ca^{2+} concentration cellular compartments," *Proc. Natl Acad. Sci. U.S.A.* **108**(39), 16265–16270 (2011).
13. A. L. Horwich et al., "The ornithine transcarbamylase leader peptide directs mitochondrial import through both its midportion structure and net positive charge," *J. Cell Biol.* **105**, 669–677 (1987).
14. K. D. Piatkevich et al., "Photoswitchable red fluorescent protein with a large Stokes shift," *Chem. Biol.* **21**(10), 1402–1414 (2014).
15. F. L. Graham and A. J. van der Eb, "A new technique for the assay of infectivity of human adenovirus 5 DNA," *Virology* **52**(2), 456–467 (1973).
16. Y. Zhao et al., "An expanded palette of genetically encoded Ca^{2+} indicators," *Science* **333**(6051), 1888–1891 (2011).
17. G. Miesenbock, D. A. De Angelis, and J. E. Rothman, "Visualizing secretion and synaptic transmission with pH-sensitive Green fluorescent protein," *Nature* **394**, 192–195 (1998).
18. T. Nagai et al., "A variant of yellow fluorescent protein with fast and efficient maturation for cell-biological applications," *Nat. Biotechnol.* **20**(1), 87–90 (2002).
19. T. Nagai et al., "Expanded dynamic range of fluorescent indicators for Ca2+ by circularly permuted yellow fluorescent proteins," *Proc. Natl Acad. Sci. U.S.A.* **101**(29), 10554–10559 (2004).
20. G. S. Baird, D. A. Zacharias, and R. Y. Tsien, "Circular permutation and receptor insertion within green fluorescent proteins," *Proc. Natl Acad. Sci. U.S.A.* **96**, 11241–11246 (1999).
21. T. Nagai et al., "Circularly permuted green fluorescent proteins engineered to sense Ca^{2+}," *Proc. Natl Acad. Sci. U.S.A.* **98**, 3197–3202 (2001).
22. J. Nakai, M. Ohkura, and K. Imoto, "A high signal-to-noise Ca^{2+} probe composed of a single green fluorescent protein," *Nat. Biotechnol.* **19**, 137–141 (2001).
23. J. Akerboom et al., "Optimization of a GCaMP calcium indicator for neural activity imaging," *J. Neurosci.* **32**(40), 13819–13840 (2012).
24. N. C. Shaner et al., "Improved monomeric red, orange and yellow fluorescent proteins derived from *Discosoma* sp. red fluorescent protein," *Nat. Biotechnol.* **22**(12), 1567–1572 (2004).
25. O. Subach et al., "A photoswitchable orange-to-far-red fluorescent protein, PSmOrange," *Nat. Methods* **8**(9), 771–777 (2011).
26. H. Tsutsui et al., "Improving membrane voltage measurements using FRET with new fluorescent proteins," *Nat. Methods* **5**(8), 683–685 (2008).
27. D. Shcherbo et al., "Far-red fluorescent tags for protein imaging in living tissues," *Biochem. J.* **418**(3), 567–574 (2009).
28. Y. P. Hung et al., "Imaging cytosolic NADH-NAD(+) redox state with a genetically encoded fluorescent biosensor," *Cell Metab.* **14**(4), 545–554 (2011).
29. S. Su et al., "Genetically encoded calcium indicator illuminates calcium dynamics in primary cilia," *Nat. Methods* **10**, 1105–1107 (2013).
30. R. K. Gupta et al., "Measurement of the dissociation constant of MgATP at physiological nucleotide levels by a combination of 31P NMR and optical absorbance spectroscopy," *Biochem. Biophys. Res. Commun.* **117**(1), 210–216 (1983).
31. A. Ikari et al., "Arachidonic acid-activated Na^+-dependent Mg^{2+} efflux in rat renal epithelial cells," *Biochim. Biophys. Acta* **1618**(1), 1–7 (2003).
32. H. C. Chen et al., "Blockade of TRPM7 channel activity and cell death by inhibitors of 5-lipooxygenase," *PLoS One* **5**(6), e11161 (2010).
33. F. I. Wolf et al., "Modulation of TRPM6 and Na^+/Mg^{2+} exchange in mammary epithelial cells in response to variations of magnesium availability," *J. Cell Physiol.* **222**(2), 374–381 (2010).
34. H. Zhou and D. E. Clapham, "Mammalian MagT1 and TUSC3 are required for cellular magnesium uptake and vertebrate embryonic development," *Proc. Natl Acad. Sci. U.S.A.* **106**(37), 15750–15755 (2009).
35. C. P. Fonseca et al., "Li^+ influx and binding, and Li^+/Mg^{2+} competition in bovine chromaffin cell suspensions as studied by 7Li NMR and fluorescence spectroscopy," *Met. Based Drugs* **7**(6), 357–364 (2000).

36. M. Schweigel et al., "Characterization of the Na^+-dependent Mg^{2+} transport in sheep ruminal epithelial cells," *Am. J. Physiol. Gastrointest. Liver Physiol.* **290**(1), G56–G65 (2006).
37. E. Murphy et al., "Monitoring cytosolic free magnesium in cultured chicken heart cells by use of the fluorescent indicator Furaptra," *Proc. Natl Acad. Sci. U.S.A.* **86**(8), 2981–2984 (1989).
38. A. I. Escobar et al., "Kinetic properties of DM-nitrophen and calcium indicators: rapid transient response to flash photolysis," *Pflügers Arch.* **434**, 615–631 (1997).
39. M. Mank and O. Griesbeck, "Genetically encoded calcium indicators," *Chem. Rev.* **108**(5), 1550–1564 (2008).
40. T. W. Hurley, M. P. Ryan, and R. W. Brinck, "Changes in cytosolic Ca^{2+} interfere with measurements of cytosolic Mg^{2+} using mag-fura-2," *Am. J. Physiol. Cell Physiol.* **263**(2), C300–307 (1992).
41. Y. Bouret, M. Argentina, and L. Counillon, "Capturing intracellular pH dynamics by coupling its molecular mechanisms within a fully tractable mathematical model," *PLoS One* **9**(1), e85449 (2014).

Vadim Pérez Koldenkova is a postdoctoral researcher at the Department of Biomolecular Science and Engineering, The Institute of Scientific and Industrial Research, Osaka University, Japan. He received his MS degree in biophysics from the Nizhny Novgorod State University, Russia, in 2003, and PhD in physiology from the University of Colima, Mexico, in 2007. His current research interests include long-distance communication in plants and application of methods of imaging for plant study.

Tomoki Matsuda is an associate professor at the Department of Biomolecular Science and Engineering, The Institute of Scientific and Industrial Research, Osaka University, Japan. He received his MS and PhD from Osaka University in 1999 and 2003, respectively. His current research interests include development of genetically encoded fluorescent indicators, methods of optical analysis, and applications of fluorescent proteins.

Takeharu Nagai is the principal investigator at the Department of Biomolecular Science and Engineering, The Institute of Scientific and Industrial Research, Osaka University, Japan. He graduated from Tsukuba University in 1992 and received his PhD from The University of Tokyo in 1998. So far, he has contributed to the invention of many fluorescent proteins. His research interests are expanding toward invention of tools for bioluminescence imaging, as well as microscopic methods for super-resolution functional imaging.